Analytical Modeling of Embedded Load Sensing Using Liquid-Filled Capillaries Integrated by Metal Additive Manufacturing

Michaël Hinderdael, Marc Moonens, Julien Ertveldt, Dieter De Baere, and Patrick Guillaume

***Abstract*— Additive manufacturing (AM) offers new manufacturing solutions for the integration of smart functionalities in engineering structures. In this paper, an analytical model is presented for an embedded load sensing element based on a liquid-filled capillary. During the additive manufacturing process, the capillary is integrated in the region where the strain is to be determined. The embedded capillary deforms as the structure deforms under an applied load, as such altering the pressure inside the capillary. The monitoring of the capillary pressure allows monitoring the loads and thus usage of the component. This paper presents a model describing the behavior of the sensing element under uniform tensile stress. The sensitivity of the load sensing element per unit longitudinal strain depends on the bulk modulus of the liquid inside the capillary and the Poisson coefficient of the surrounding material. The current work further compares the analytical model against static tension-compression tests of powder bed fused stainless steel (AISI 316L) test specimen with an integrated capillary filled with a liquid (water). Similarly, the validation of the model is then checked against a dynamic four-point bending test on a Ti-6Al-4V specimen produced by powder bed fusion.**

***Index Terms*— Additive manufacturing, embedded load sensing, usage monitoring, structural health monitoring, effective structural health monitoring.**

I. Introduction

SMART structures are capable of detecting the presence of damage and measuring the loads that are acting upon them. Such information can be used to estimate the global health condition of the structure, compare the effective loads with the design loads and forecast the remaining useful lifetime (RUL) of the structure under analysis. With the invention of novel manufacturing techniques (e.g. composites and additive manufacturing (AM)) the capability of integrating sensors came along. The future generation of Structural Health Monitoring (SHM) and Usage Monitoring (UM) technologies will be based on sensor technology directly integrated in the material during the manufacturing process [6]. The attractive potential of such integrated technologies arise from the added value in terms of more reliable damage monitoring systems, reduced inspection monitoring cost and improved safety [28, p.65]. Such an integrated solution is especially more robust and reliable because of its inherent protection against environmental changes, accidental damage and ingress of oil, dirt and other contaminants.

The layerwise addition of material during the additive manufacturing process enables function integration such as an embedded SHM sensor. Research is ongoing to integrate electrical conductors inside AM polymers to generate built-in sensors. Liquid metal is being inserted in 3D printed microchannels [17], [19], [31]. Strain gauges have been printed in conductive ink on top of a structure [20] and inside highly stretchable elastomers [1], [16]. Despite their successful operation, many drawbacks have been reported on the use of conductive ink. The curing must happen at an elevated temperature and for a significant amount of time, which might be incompatible with the polymers commonly used in 3D printing. The process is also too costly for large scale production. Furthermore, this concept cannot be extended to metallic, i.e. conductive components. The conductive ink is also approximately 100 times more expensive than ordinary copper, but its conductivity is commonly 30 times less. Therefore, researchers have begun to explore the use of solid metal conductors, such as copper wires, in polymer 3D printing [20], [26]. Scheyer and Anton employed the electromechanical impedance (EMI) method on piezoelectric transducers embedded inside AM parts to evaluate the feasibility of performing SHM on parts fabricated using additive manufacturing [22].

Saheb and Mekid provided a review of methods for the integration of optical fibers for sensing applications in metals with the inclusion of additive manufacturing [21]. Fiber-optic strain sensors are being embedded in metals by means of powder-bed based additive manufacturing [12], [13], shape deposition manufacturing [10], [11] and ultrasonic additive manufacturing [9], [15], [23].

A different way of creating smart materials consists in the monitoring of the pressure level inside capillaries that were integrated during the manufacturing process. This novel concept is called the effective Structural Health Monitoring (eSHM) principle. Initially, the principle was utilized to detect fatigue cracks in metals processed using powder-bed-fusion [30] and directed energy deposition [29], but has more recently been extended to measure strains [7]. The concept of

Manuscript received May 17, 2019; revised June 24, 2019; accepted June 24, 2019. Date of publication June 26, 2019; date of current version September 18, 2019. This work was supported by the Agency for Innovation by Science and Technology in Flanders (IWT) under Grant 141.067. The associate editor coordinating the review of this paper and approving it for publication was Dr. Camilla Baratto. *(Corresponding author: Michaël Hinderdael.)*

The authors are with the Department of Mechanical Engineering, Vrije Universiteit Brussel, 1050 Brussels, Belgium (e-mail: michael.hinderdael@vub.be; marc.moonens@vub.be; julien.ertveldt@vub.be; dieter.de.baere@vub.be; patrick.guillaume@vub.be).

Digital Object Identifier 10.1109/JSEN.2019.2925206

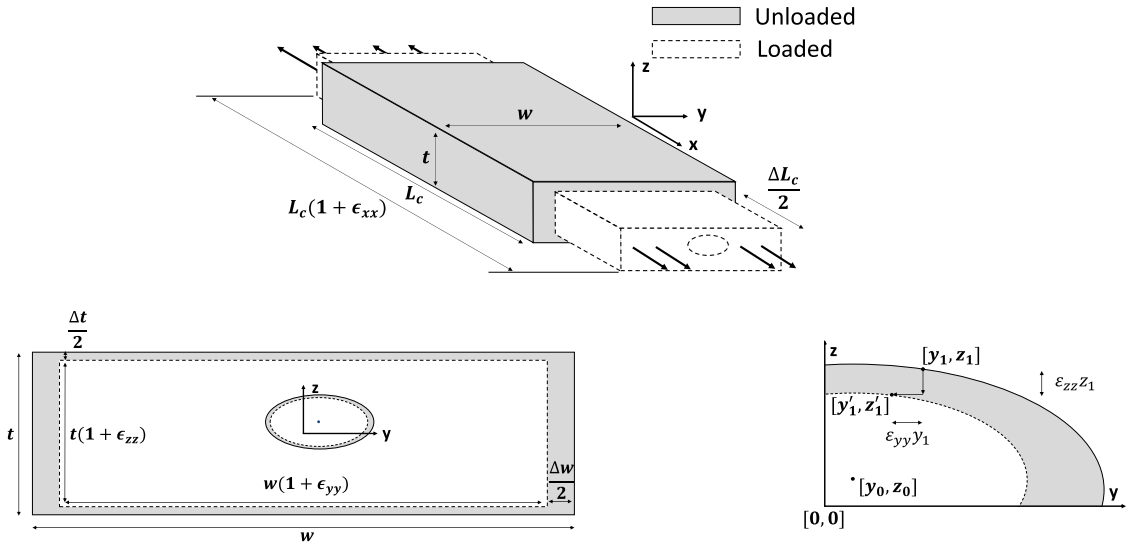

Fig. 1. Analytical model of a tensile stressed cross section with integrated capillary for usage monitoring.

this novel load monitoring principle has been demonstrated on ABS polymer tensile test specimens with integrated capillaries filled with air and water. As was concluded by the authors, the lack of repeatability and the limited usable lifetime of the presented load monitoring principle was caused by the nature of the selected material (polymer ABS). It was concluded that a future test campaign on metallic tensile test specimens with an integrated capillary should be conducted. Since the use of a liquid (water), instead of a gas (air), resulted in a more sensitive load sensing mechanism, the current work further explores the capabilities of the load sensing element using a liquid (water) inside the capillary.

In the following part of the manuscript, the concept of strain sensing through the integration of liquid-filled capillaries inside the structure is studied. The deformation of the capillary and the resulting pressure change inside the capillary is first analyzed through an analytical study. Such a model allows determining the most important parameters affecting the sensitivity of this strain sensing principle. The analytical model will then be validated on the basis of a quasi-static tension compression and a dynamic four-point bending test campaign on metallic tensile test specimens produced with additive manufacturing. All presented test results concern capillaries that were filled with water.

II. Analytical Model

The analytical model will predict the pressure change inside a capillary integrated in the cross section of a tensile test specimen with a width w and thickness t, as shown in Fig. 1. The analysis is conducted for capillaries with an elliptical cross section (which includes the special and most popular case of a circular capillary).

Fig. 1 presents a tensile specimen which will be used as a model for the analytical derivation of the pressure variation expected inside an elliptical capillary during a tension-compression test. Assuming small strains and small displacements, a tensile load acting on the tensile specimen will elongate the specimen in the x-direction:

$$\frac{L_{c,l}}{L_c} = (1 + \epsilon_{xx}) \tag{1}$$

with L_c the initial length of the test section in which the capillary is embedded, $L_{c,l}$ representing the length of the test section after application of the load and ϵ_{xx} the longitudinal strain. This action is elongating the capillary, thereby increasing the capillary volume. Consequently, the capillary pressure will drop. The Poisson effect limits the capillary volume increase since the cross sectional area of the test specimen, and thus also that of the capillary, will decrease. The rate at which the cross sectional dimensions decrease with the applied tensile strain is given by the Poisson coefficients ν_{xy} and ν_{xz}.

$$\epsilon_{yy} = -\nu_{xy}\epsilon_{xx} \tag{2}$$

$$\epsilon_{zz} = -\nu_{xz}\epsilon_{xx} \tag{3}$$

in which ϵ_{yy} and ϵ_{zz} are transversal strains in the y and z direction respectively. With the axis defined as in Fig. 1, thus with the origin of the axis at the planes of symmetry of the test specimen, any point $[x, y, z]$ of the cross section subjected to a uniform stress ϵ_{xx} will displace to $[x', y', z']$ in the following manner:

$$x' = \epsilon_{xx} x \tag{4}$$

$$y' = \left(1 + \epsilon_{yy}\right) y = \left(1 - \nu_{xy}\epsilon_{xx}\right) y \tag{5}$$

$$z' = (1 + \epsilon_{zz})\, z = (1 - \nu_{xz}\epsilon_{xx})\, z \tag{6}$$

Considering the case of pure tension, all points that are located on a plane at a given distance x in the unloaded case will remain on a plane and translate to the plane x' when loaded. On any given cross section of the tensile specimen, a point $[x, y_1, z_1]$ located on an ellipse (e.g. the capillary

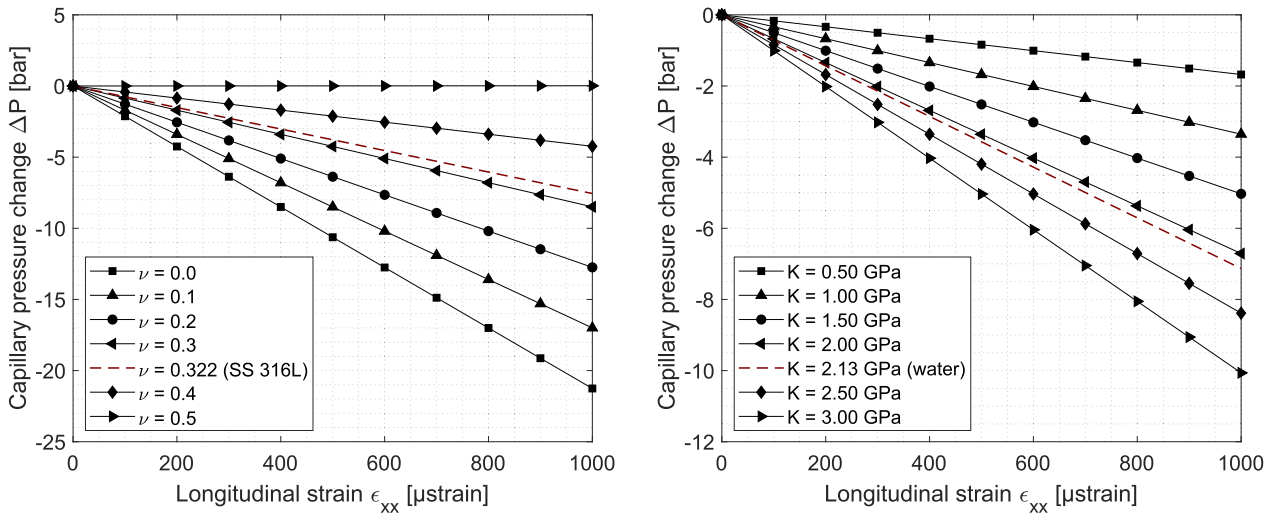

Fig. 2. The influence of **(a)** the Poisson coefficient ν and **(b)** the bulk modulus K on the sensitivity of load sensing element. The analysis is based on the analytical model with the dashed line representing the practical test case (stainless steel $\nu = 0.322$, water $K = 2.13$ GPa and $V_{c\%} = 100\%$).

surface) with radius's r_1 and r_2 and the center of the ellipse positioned at $[x, y_0, z_0]$ satisfies the equation:

$$\left(\frac{(y_1 - y_0)}{r_1}\right)^2 + \left(\frac{(z_1 - z_0)}{r_2}\right)^2 = 1 \tag{7}$$

With the application of a uniform tensile load and longitudinal strain ϵ_{xx}, all points on the ellipse remain on an ellipse with radiuses r_1' and r_2' and its center located at $[y_0', z_0']$:

$$r_1' = \left(1 - \nu_{xy}\epsilon_{xx}\right) r_1 \tag{8}$$

$$r_2' = \left(1 - \nu_{xz}\epsilon_{xx}\right) r_2 \tag{9}$$

$$y_0' = \left(1 - \nu_{xy}\epsilon_{xx}\right) y_0 \tag{10}$$

$$z_0' = \left(1 - \nu_{xz}\epsilon_{xx}\right) z_0 \tag{11}$$

After deformation, the new cross sectional area $A_{c,l}$ of the ellipse equals

$$A_{c,l} = \left(1 - \nu_{xy}\epsilon_{xx}\right)\left(1 - \nu_{xz}\epsilon_{xx}\right) A_c \tag{12}$$

$$V_{c,l} = \left(1 - \nu_{xy}\epsilon_{xx}\right)\left(1 - \nu_{xz}\epsilon_{xx}\right)\left(1 + \epsilon_{xx}\right) V_c \tag{13}$$

where A_c represents the initial, unloaded, cross sectional area of the capillary. The Poisson effect counteracts the volumetric increase of the capillary volume due to the longitudinal elongation ϵ_{xx} by reducing the cross sectional area of the capillary. The larger the Poisson coefficient, the smaller the cross section of the resulting capillary. The Poisson coefficients ν_{xy} and ν_{xz} will have to be determined independently for non-voxel based AM techniques and formula (13) will have to be used in the remainder of the derivation hereafter (e.g. line-based AM techniques such as Directed Energy Deposition (DED) and Fused Deposition Modeling (FDM)). However, given the voxel based AM technique being used and with the build direction along the x-axis, the material can be considered quasi-isotropic in the yz-plane with the Poisson coefficient $\nu_{xy} = \nu_{xz} = \nu$. This assumption simplifies the equation (13) to:

$$A_{c,l} = (1 - \nu\epsilon_{xx})^2 A_c \tag{14}$$

$$V_{c,l} = (1 - \nu\epsilon_{xx})^2 (1 + \epsilon_{xx}) V_c \tag{15}$$

To determine the pressure variation ΔP inside the capillary due to a tensile load on the tensile specimen, it suffices to express the definition of the bulk modulus K:

$$\Delta P = -K \frac{\Delta V_c}{V_t} \tag{16}$$

The pressure change as a result of the volume change inside the capillary $\Delta V_c = V_{c,l} - V_c$ is evenly distributed over the total fluid volume V_t, being the combined volume of the capillary and the fluid volume in between the capillary and the connectors.

$$\Delta P = -K \frac{V_{c,l} - V_c}{V_c} V_{c\%} \tag{17}$$

in which ΔV_c represents the capillary volume change, V_c the capillary volume in unloaded condition and $V_{c\%} = \frac{V_c}{V_t}$ the capillary volume fraction. With the inclusion of equation (15), the pressure variation inside the capillary becomes:

$$\Delta P = K \left(1 - (1 - \nu\epsilon_{xx})^2 (1 + \epsilon_{xx})\right) V_{c\%} \tag{18}$$

In the special case of the more common circular capillary ($r_1 = r_2 = R$), the same derivation can be done and results in the same equation, Equation (18). Considering that the strain ϵ_{xx} remains small, one can simplify the equation by neglecting second order terms:

$$\Delta P = K\,(2\nu - 1)\,\epsilon_{xx} V_{c\%} \tag{19}$$

The pressure output of the sensing element is linearly depending on the applied strain and the sensitivity $\frac{\Delta P}{\epsilon_{xx}}$ is linearly depending on the Poisson coefficient ν, bulk modulus K and capillary fraction $V_{c\%}$. The following sections will shortly discuss the importance of the parameters influencing the sensitivity of the load sensing element.

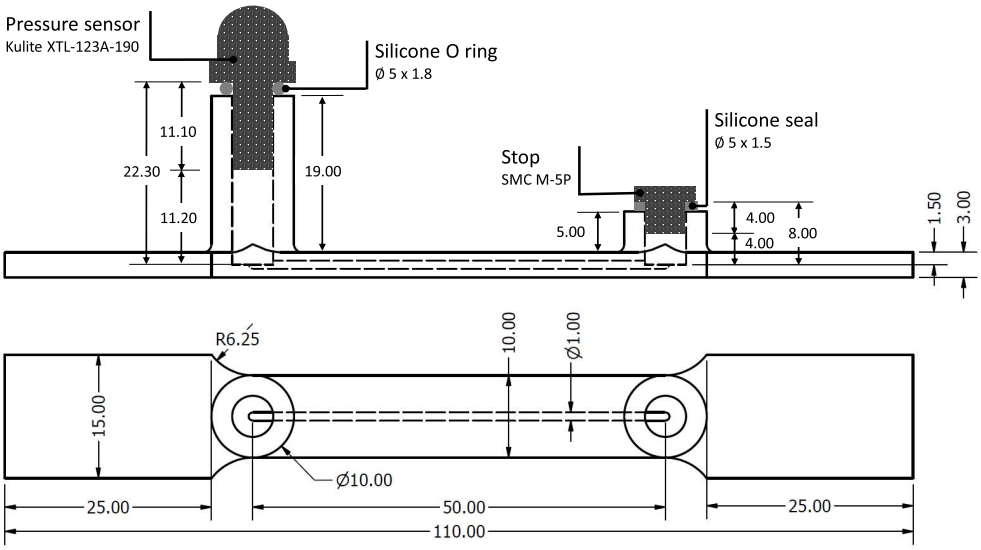

Fig. 3. Dimensions of the metal additive manufactured tensile test specimen (in mm).

A. Shape, Size and Position of the Capillary

This analytical development shows that neither the actual shape (ellipse or circle), nor the size (the radiuses) and position of the capillary do influence the sensitivity of the pressure signal inside the capillary when subjected to a uniform longitudinal strain ϵ_{xx}. Only the relative size of the capillary with respect to the total liquid volume $V_{c\%}$ influences the sensitivity of the overall system.

B. Poisson Coefficient ν

This development furthermore clearly shows the importance of the Poisson coefficient, naturally limited between $0 < \nu < 0.5$, although smart designs using additive manufacturing allow creating auxetic structures [24], [32]. A smaller or negative Poisson coefficient leads to a larger pressure signal for a given elongation while a Poisson coefficient of 0.5 does not induce any pressure variation inside the capillary. The effect of the Poisson coefficient on the pressure signal inside the capillary due to the volumetric change of the capillary is depicted in Fig. 2 **(a)** for capillaries filled with water.

The Poisson coefficient cannot really be seen as a design parameter. It is a material parameter and the material is most frequently fixed by other design requirements. The Poisson coefficient furthermore has a limited range in which it can be varied, with most materials having a Poisson coefficient ranging between 0.25 to 0.4, although exceptions and new design solutions can result in Poisson coefficients even outside the 'natural' limits of $0 < \nu < 0.5$.

C. Bulk Modulus K

The single design parameter influencing the sensitivity of the load sensing element is the bulk modulus K of the fluid inside the capillary. The higher the bulk modulus, the larger the pressure variations expected inside the capillary. Fig. 2 **(b)** presents the capillary pressure variations for different theoretical bulk modulus values. The bulk modulus of water has been studied in various independent works [2], [4] which were summarized to an average bulk modulus $\bar{K} = 2.1257$ GPa and a maximum spread of $|\Delta K| = 0.0531$ GPa.

III. Static Tension-Compression Test

A. Design

The design of the tensile test specimen is depicted in Fig. 3. The capillary is embedded in the tensile test section of the test specimen. A connector is foreseen at either side of the capillary, allowing the liquid to flow through the capillary to ensure complete filling. One of the connectors has been elongated to avoid that the pressure sensor is installed in a region of stress concentrations around the connector, thereby avoiding erroneous pressure recordings. The length of the specimen was shortened to a minimum to reduce the production cost which is directly proportional to the build height. In view of practical applications, the capillary diameter was minimized to reduce the impact on the component, while currently being limited at $D = 1$mm to allow powder removal. After installation of the pressure sensor (Kulite XTL-123A-190, Kulite Semiconductor Products, Inc., Leonia, USA) with a thread length of 10.1 mm and the stop screw (M-5P, SMC Corporation, Chiyoda, Tokio, Japan) at the second connector end, the sensing capillary volume fraction equals:

$$V_{c\%} = \frac{\pi 0.5^2 50}{\pi 0.5^2 50 + \pi 2.5^2((22.3 - 11.1) + (8 - 4))} = 11.6\% \quad (20)$$

B. Production Process and Material Properties

1) Production Process: The tensile test specimens were produced with laser based Powder Bed Fusion (PBF). This additive manufacturing technique is currently the most widespread metal additive manufacturing technique. Its high geometrical accuracy allows producing small tensile specimens

with integrated capillaries for the conduction of this tensile test campaign. The tensile test specimens were produced in stainless steel AISI 316L. The built direction was vertical (along the x axis in Fig. 1). Contours were first scanned at 500 $\frac{\text{mm}}{\text{s}}$ with a laser power of 80 W while hatching occurred at 675 $\frac{\text{mm}}{\text{s}}$ at a laser power of 150 W. The hatch spacing was 80 μm and layer thickness was 20 μm. The powder particles of the powder bed have a particle size distribution between 15-40 μm. In order to limit oxidation, the oxygen content inside the built chamber was lowered to 0.1% and shielding gas at a flow speed of 2.5 $\frac{\text{m}}{\text{s}}$ furthermore prevented oxygen from entering the area of molten metal. After production, the loose metal particles of the powder bed inside the capillary were removed using pressurized air.

2) Material Properties: AISI SS316L Produced by Laser Based PBF: Before discussing the sensitivity of the sensing element, the Young Modulus and Poisson coefficient of the additively manufactured specimens were determined. The latter material parameters were determined during a tensile test on two specimens with a similar design as depicted in Fig. 3, except that no capillary nor connections were foreseen on the specimen. The test specimens had a dog bone shape with two-element 90° planar rosette strain gauges installed at both sides of the test specimen. Each specimen was tested three times. For each individual test, the material parameters were obtained by averaging out the result between the front and the back rosette strain gauge of the specimen as reported in the table in Fig. 4.

Fig. 4 **(a)** presents the averaged stress-strain curve for Specimen 1 and Specimen 2. The average Young modulus of the additively manufactured AISI 316L stainless steel is $\bar{E} = 146.7$ GPa, which compares to well-known values from the literature [8]. The average Poisson coefficient of Specimen 1 and Specimen 2 were respectively 0.315 and 0.329. The Poisson coefficient considered in this paper is therefore the average of these two specimens, $\bar{\nu} = 0.322$ with largest measured deviation $|\Delta\nu| = 0.01$. Fig. 5 **(a)** presents the tensile test specimen in the test setup for the determination of the Poisson coefficient using strain gauges.

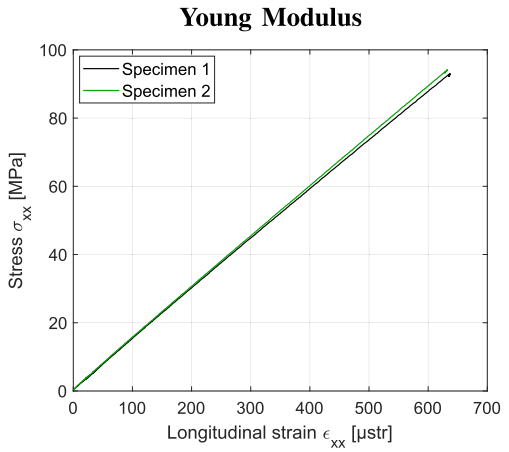

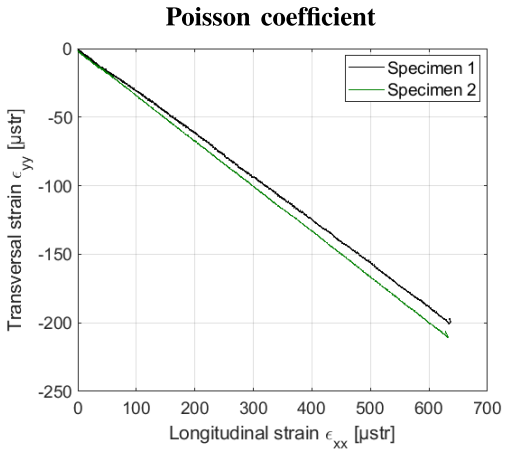

	Specimen 1		Specimen 2	
	E [GPa]	ν[-]	E [GPa]	ν[-]
1	145.5	0.315	146.5	0.327
2	145.5	0.312	148.5	0.331
3	146.1	0.317	148.2	0.328
avg.	145.7	0.315	147.7	0.329

Fig. 4. Tensile test results to determine Young Modulus and Poisson Coefficient of the 316L stainless steel test specimens produced using laser based Powder Bed Fusion.

C. Testing

After production, the specimen was submerged in a tank filled with tap water and placed in a vacuum oven to avoid the presence of air bubbles inside the capillary. The pressure sensor and stop were then installed on the test specimen. Care should be taken in this phase to avoid pressure rises exceeding the range of the pressure sensor. The use of an anaerobic thread sealant (e.g. Loctite 577, Henkel, Düsseldorf, Germany), that only cures in oxygen free conditions, initially provides sufficient permeability to prevent high pressure build-ups when connecting the pressure sensor and stop. An additional O-ring assists in sealing the threaded connections. The tensile test samples were placed in an Instron 5885 H (Instron, Norwood, USA) tensile testing machine with Instron 2518-103 load cell (10 kN static). An Instron 2630-030 extensometer was furthermore installed on the test section. The pressure sensor, extensometer, load cell and cross head displacement were all recorded using an LMS Scadas III mobile data acquisition system (Siemens, Munich, Germany). All channels were synchronously sampled at a rate of 6.4 kHz. Fig. 5 **(b)** shows the setup.

D. Results

Fig. 6 presents an example of the test result while the table presents five measurements conducted on the same test specimen. The capillary pressure is presented against the strain inside the specimen which can be generalized to other cases. For completeness, the top x-axis furthermore presents the loading condition that corresponds to these strain levels for this particular design. The test was conducted both under tension and compression. The initial pressure level slightly varied in between different tests.

As expected from the analytical model, the pressure varies nearly linear with respect to the strain. The average sensitivity obtained during this test campaign was $-83.2\ \frac{\text{Pa}}{\mu\text{strain}}$ which compares quite well with the analytically expected

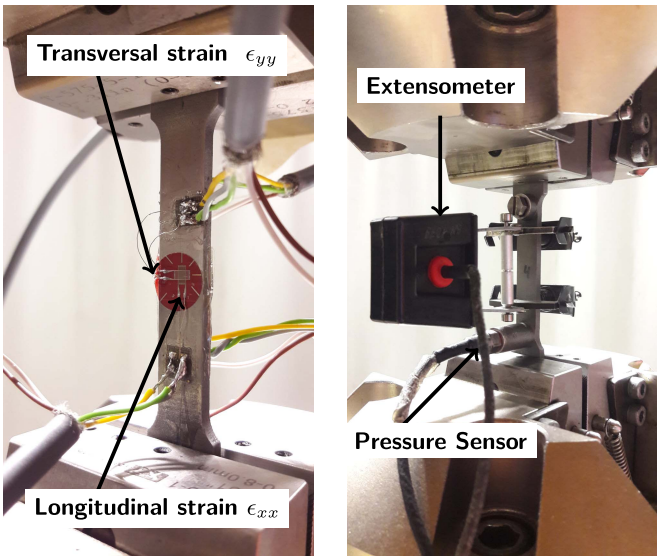

Fig. 5. (a) Detailed view of the two strain measurements (longitudinal and transversal) through strain gauges for the determination of the Poisson coefficient of the additive manufactured AISI 316L. (b) Detailed view on the tensile test setup with a strain measurement through the extensometer and the pressure sensor connected to the integrated capillary of the eSHM system.

sensitivity:

$$\frac{\Delta P}{\epsilon_{xx}} = \bar{K}\,(2\bar{\nu}-1)\,V_{c\%} = -87.8 \pm 8.8 \quad \frac{\text{Pa}}{\mu\text{strain}} \tag{21}$$

It can be concluded that the proposed analytical model is capable of predicting the sensitivity of the embedded strain sensing element. The determining parameters affecting the sensitivity of the embedded sensing element have been identified. The resolution of the strain measurement is determined based on the noise level of the pressure sensor being used. For this particular test, 99.73% of all errors due to noise remain within a band of 3.9 Pa (3σ), therefore having a signal-to-noise ratio S/N $= 10\log\frac{170{,}000\text{Pa}}{3.9\text{Pa}} = 46.4$dB. In this configuration, the eSHM strain sensing element can therefore determine the strain level with a resolution well below 1 μstrain (here 0.044 μstrain). The performance of this highly linear, high sensitive eSHM load sensing concept can therefore compete with conventional strain gauges that are externally applied and may be compared against other embedded load/strain sensors [1], [13], [14]

IV. Dynamic Four-Point Bending Test

A. Design

The developed model has been furthermore validated against a dynamic four-point bending test to furthermore demonstrate the capability of the system to follow dynamic load conditions. The design of the four-point bending test specimen is presented in Fig. 7. The connections for the pressure sensor and stop are located outside the outer rollers as bending stresses are there reduced to zero, avoiding potential erroneous pressure recordings. With the pressure sensor (Kulite XTL-HA-123G-190M-7-bara, Kulite Semiconductor

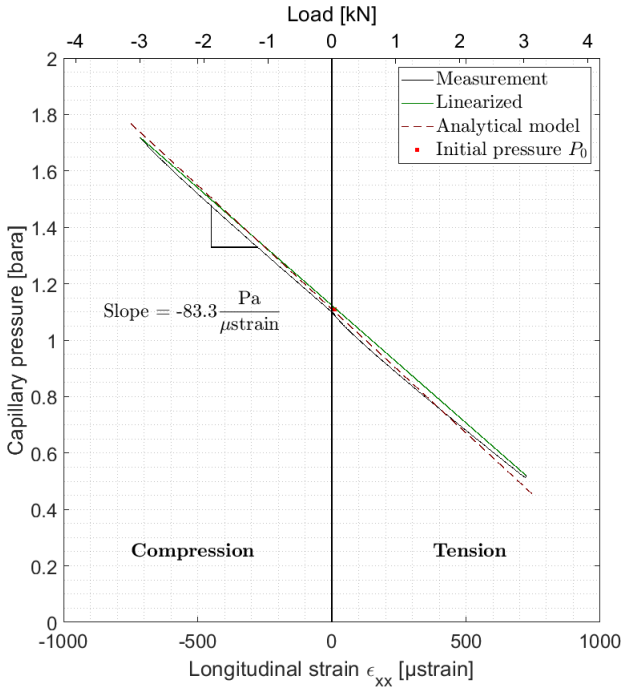

Test	P_0 [bara]	Slope [Pa/μstrain]
1	1.11	-83.3
2	1.12	-84.0
3	1.20	-82.8
4	1.21	-83.1
5	1.22	-83.0
avg.		-83.2

Fig. 6. Tensile and compression test on a stainless steel 316L dog bone test specimen with an integrated capillary filled with water. The capillary pressure is linear with respect to the longitudinal strain, both under tension and compression (top). Multiple test results are presented and compared in the table (bottom).

Products, Inc., Leonia, USA) and stop screw (M-5P, SMC Corporation, Chiyoda, Tokio, Japan) in place, the sensing fraction of the capillary equals:

$$\begin{aligned} V_{c\%} &= \frac{\pi 0.60^2 100}{\pi 0.60^2 100 + \pi 2.5^2((9.00-5.28)+(8.50-4.00))} \\ &= 41.2\% \end{aligned} \tag{22}$$

In longitudinal direction, the straight capillary senses the average of the typical strain profile of a four point bending configuration, starting from zero at the outer rollers and linearly rising to a maximum at the inner rollers and being constant in between the inner rollers. That average of the strain profile, as sensed by the capillary, is given by:

$$\bar{\epsilon}_{xx} = \frac{\frac{L}{4}\frac{\epsilon_{xx,max}}{2} + \frac{L}{2}\epsilon_{xx,max} + \frac{L}{4}\frac{\epsilon_{xx,max}}{2}}{L} = \frac{3}{4}\epsilon_{xx,max} \tag{23}$$

with L being the length between the outer rollers and $\frac{L}{2}$ and $\frac{L}{4}$ respectively the distances between the inner rollers and

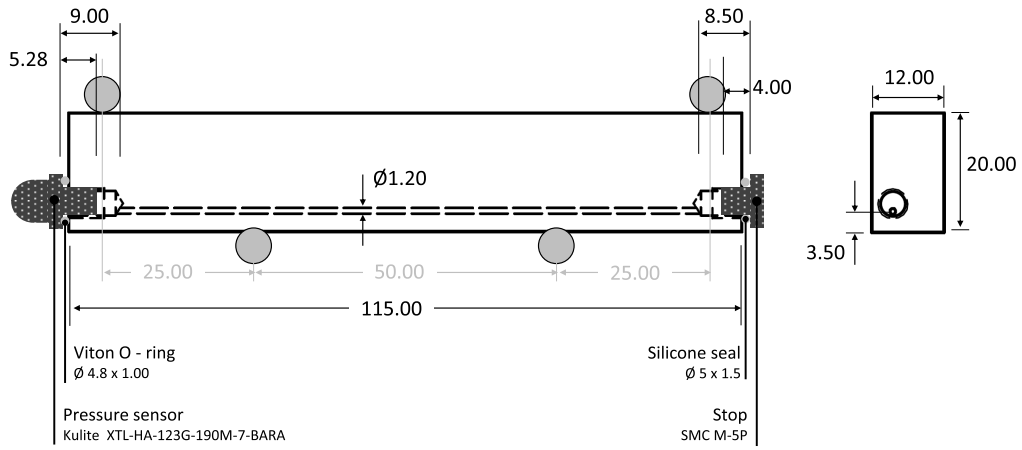

Fig. 7. Dimensions of the metal additive manufactured four point bending test specimen (in mm).

between an inner and outer roller. $\epsilon_{xx,max}$ furthermore being the theoretical maximum strain as found on the outer edge of the specimen between the inner rollers. It is the average strain $\bar{\epsilon}_{xx}$ that now should be used to predict the pressure change inside the load sensing element and should therefore be used in equation (19).

B. Production Process and Material Properties

The four point bending test specimen was ordered at 3D systems (3D Systems, Rock Hill, SC, USA) without access to the process parameters. The Ti-6Al-4V specimen has been built in the vertical direction with a layer thickness of 30μm and has been post-processed using a Hot-Isostatic-Pressing (HIP) to reduce porosity and material anisotropy and remove residual stresses. The specimen has furthermore been treated with a chemical etching process to reduce capillary surface roughness. Based on previous works, the Poisson coefficient of Ti-6Al-4V produced by PBF is found to be 0.32 [25] and 0.324 [27] which summarizes at an average of $\bar{\nu} = 0.322$. Similarly, the Young Modulus of HIPped Ti-6Al-4V produced by means of PBF is found to be 115.4 GPa [3] and 114 GPa [5], which for this work is averaged to $\bar{E} = 114.7$ GPa.

C. Testing

Similarly to the tensile test specimen, also the four point bending test specimen was submerged in a tank filled with tap water and placed in a vacuum oven to avoid the presence of air bubbles inside the capillary. The pressure sensor and stop were then installed on the test specimen before being placed in the four point bending test setup. The specimen was then loaded with an amplitude of 9.3 kN around a mean load level of 15 kN with a frequency of 15 Hz. The pressure sensor, load cell and cross head displacement were recorded using an LMS Scadas III mobile data acquisition system (Siemens, Munich, Germany). All channels were synchronously sampled at a rate of 40.96 kHz.

D. Results

Fig. 8 presents an example of five consecutive cycles of the four bending test. The capillary pressure is again presented against the averaged strain expected over the entire length of the capillary. For completeness, the top x-axis furthermore presents the loading condition that corresponds to these strain levels for this particular design. along with the analytical model predicting the sensitivity of the load sensing element:

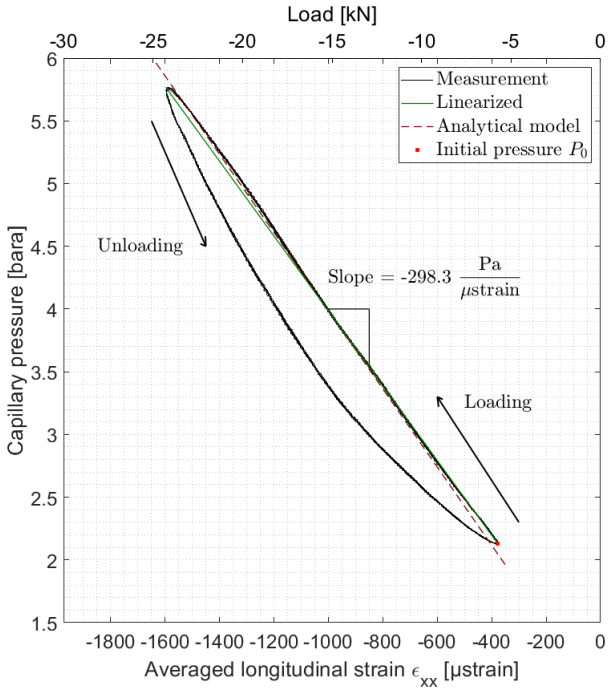

Fig. 8. Dynamic four point bending test on a Ti-6Al-4V beam with an integrated straight capillary under compression, filled with water. The capillary pressure is linear with respect to the averaged longitudinal strain, although hysteresis is clearly present.

$$\frac{\Delta P}{\epsilon_{xx}} = \bar{K}\,(2\bar{\nu}-1)\,V_{c\%} = -311.8 \;\pm 11.0\;\frac{\text{Pa}}{\mu\text{strain}} \quad (24)$$

The analytically derived model is well capable to predict the sensitivity of the load sensing element. The test results show the presence of hysteresis which is also present in the load-displacement and pressure-displacement plots, as depicted in Fig. 9 for 25 consecutive cycles. This effect is likely a consequence of frictional effects between the

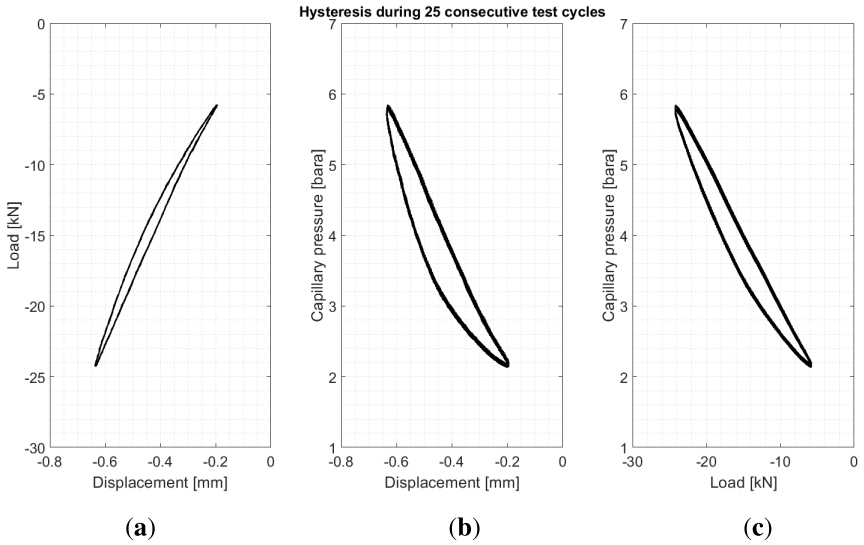

Fig. 9. The dynamic four point bending test shows hysteresis behavior in the (**a**) Displacement-Load, (**b**) Displacement-Pressure and (**c**) Load-Pressure plots.

rollers and specimen [18]. The sensitivity is now larger when compared to the tensile test configuration, which is a direct result of the larger capillary volume fraction $V_{c\%}$. The liquid inside the capillary and the Poisson coefficient of the material being used were the same in both configurations.

V. Conclusions

The current work has presented an analytical model predicting the sensitivity of the embedded eSHM system acting as a load sensing element inside additively manufactured parts. The embedded sensing technology is based on the pressure monitoring inside capillaries that were integrated during the production process of the specimens. The deformation of the test specimen under the applied loads induces capillary volume changes that, in turn, alter the pressure inside the capillary. The capillaries were filled with an incompressible fluid (water) in order to increase sensitivity.

The model that has been presented, indicated that a very sensitive embedded sensor can be obtained. The bulk modulus of the fluid inside the capillary and the Poisson coefficient of the surrounding material are the two important material properties that influence the sensitivity of the system. The measured sensitivity during a tension-compression test campaign on AISI 316L stainless steel specimens produced using laser based Powder Bed Fusion technology was in good comparison with the theoretically derived sensitivity.

The model has been furthermore compared against a four point bending test condition under dynamic loading at 15 Hz. The predicted sensitivity again compared well against the measured one and the pressure recording could easily follow the dynamic loading.

The current work has proven the concept of embedded strain sensing using liquid-filled capillaries within metallic test specimens. An analytical model predicting the sensitivity of the system has been proposed and the experimental results prove the high sensitivity of the embedded strain sensing technology. The average strain level over the capillary length can be estimated with a resolution smaller than 1 μstrain and can therefore compete with conventional strain gauges that are externally applied to the surface.

Annex

Fig. 9 shows the hysteresis behavior during the four-point bending test in the Displacement-Load, Displacement-Pressure and Load-Pressure plots.

References

[1] S. Agarwala *et al.*, "Development of bendable strain sensor with embedded microchannels using 3d printing," *Sens. Actuators A, Phys.*, vol. 263, pp. 593–599, Aug. 2017.

[2] A. Bahadori and B. H. Vuthaluru, "Prediction of bulk modulus and volumetric expansion coefficient of water for leak tightness test of pipelines," *Int. J. Pressure Vessels Piping*, vol. 86, no. 8, pp. 550–554, Aug. 2009.

[3] A. M. Beese and B. E. Beth, "Review of mechanical properties of Ti-6Al-4V made by laser-based additive manufacturing using powder feedstock," *JOM*, vol. 68, no. 3, pp. 724–734, Mar. 2015.

[4] R. A. Fine and F. J. Millero, "Compressibility of water as a function of temperature and pressure," *J. Chem. Phys.*, vol. 59, no. 10, pp. 5529–5536, Sep. s1973.

[5] J. Günther, "On the effect of internal channels and surface roughness on the high-cycle fatigue performance of ti-6al-4v processed by SLM," *Mater. Des.*, vol. 143, pp. 1–11, Apr. 2018.

[6] I. Herszberg, M. K. Bannister, H. C. Li, R. S. Thomson, and C. White, "Structural health monitoring for advanced composite structures," in *Proc. 16th Int. Conf. Compos. Mater.*, Jun. 2007, pp. 1–13.

[7] M. Hinderdael *et al.*, "Proof of concept of integrated load measurement in 3D printed structures," *Sensors*, vol. 17, no. 2, pp. 1–12, Feb. 2017.

[8] L. Hitzler *et al.*, "On the anisotropic mechanical properties of selective laser-melted stainless steel," *Materials*, vol. 10, no. 10, p. 1136, Sep. 2017.

[9] J. Li, T. Monaghan, S. Masurtschak, A. Bournias-Varotsis, R. J. Friel, and R. A. Harris, "Exploring the mechanical strength of additively manufactured metal structures with embedded electrical materials," *Mater. Sci. Eng., A*, vol. 639, pp. 474–481, Jul. 2015.

[10] X. Li and F. Prinz, "Embedding of fiber optic sensors in layered manufacturing," in *Proc. Solid Freeform Fabr. Symp.*, Aug. 2003, pp. 314–324.

[11] X. Li, "Embedded sensors in layered manufacturing," Ph.D. dissertation, Dept. Mech. Eng., Stanford Univ., Stanford, CA, USA, 2001.

[12] P. Stoll *et al.*, "Embedding fibre optical sensors into SLM parts," in *Proc. 27th Annu. Int. Solid Freeform Fabr.*, 2016, pp. 1815–1825.

[13] R. R. J. Maier *et al.*, "Embedded fiber optic sensors within additive layer manufactured components," *IEEE Sensors J.*, vol. 13, no. 3, pp. 969–979, Mar. 2013.
[14] A. A. S. Mohammed, W. Moussa, and E. Lou, "High sensitivity MEMS strain sensor: Design and simulation," *Sensors*, vol. 8, no. 4, pp. 2642–2661, Apr. 2008.
[15] T. Monaghan, A. J. Capel, S. D. Christie, R. A. Harris, and R. J. Friel, "Solid-state additive manufacturing for metallized optical fiber integration," *Compos. A, Appl. Sci. Manuf.*, vol. 76, pp. 181–193, Sep. 2015.
[16] J. T. Muth *et al.*, "Embedded 3D printing of strain sensors within highly stretchable elastomers," *Adv. Mater.*, vol. 26, no. 36, pp. 6307–6312, Sep. 2014.
[17] H. Ota *et al.*, "Application of 3D printing for smart objects with embedded electronic sensors and systems," *Adv. Mater. Technol.*, vol. 1, no. 1, Apr. 2016, Art. no. 1600013.
[18] W. Van Paepegem, K. De Geyter, P. Vanhooymissen, and J. Degrieck, "Effect of friction on the hysteresis loops from three-point bending fatigue tests of fibre-reinforced composites," *Compos. Struct.*, vol. 72, no. 2, pp. 212–217, Feb. 2006.
[19] Y.-L. Park, C. Majidi, R. Kramer, P. Bérard, and R. J. Wood, "Hyperelastic pressure sensing with a liquid-embedded elastomer," *J. Micromech. Microeng.*, vol. 20, no. 12, Nov. 2010, Art. no. 125029.
[20] M. Saari, B. Cox, E. Richer, S. P. Krueger, and L. A. Cohen, "Fiber encapsulation additive manufacturing: An enabling technology for 3D printing of electromechanical devices and robotic components," *3D Printing Additive Manuf.*, vol. 2, no. 1, pp. 32–39, Mar. 2015.
[21] N. Saheb and S. Mekid, "Fiber-embedded metallic materials: From sensing towards nervous behavior," *Materials*, vol. 8, no. 12, pp. 7938–7961, Nov. 2015.
[22] A. G. Austin and S. R. Anton, "Impedance-based structural health monitoring of additive manufactured structures with embedded piezoelectric wafers," *Proc. SPIE*, vol. 10168, Apr. 2017, Art. no. 1016827.
[23] J. J. Schomer, "Embedding fiber Bragg grating sensors through ultrasonic additive manufacturing," M.S. thesis, Dept. Mech. Eng., Ohio State Univ., Columbus, OH, USA, 2017.
[24] J. Schwerdtfeger, P. Heinl, R. F. Singer, and C. Körner, "Auxetic cellular structures through selective electron-beam melting," *Phys. Status Solidi*, vol. 247, no. 2, pp. 269–272, Feb. 2010.
[25] A. Z. Senalp, O. Kayabasi, and H. Kurtaran, "Static, dynamic and fatigue behavior of newly designed stem shapes for hip prosthesis using finite element analysis," *Mater. Des.*, vol. 28, no. 5, pp. 1577–1583, 2007.
[26] C. Shemelya *et al.*, "Encapsulated copper wire and copper mesh capacitive sensing for 3-D printing applications," *IEEE Sensors J.*, vol. 15, no. 2, pp. 1280–1286, Feb. 2015.
[27] M. Simonelli, Y. Y. Tse, and C. Tuck, "Effect of the build orientation on the mechanical properties and fracture modes of SLM Ti–6Al–4V," *Mater. Sci. Eng., A*, vol. 616, pp. 1–11, Oct. 2014.
[28] W. Staszewski, C. Boller, and G. R. Tomlinson, *Health Monitoring of Aerospace Structures: Smart Sensor Technologies and Signal Processing*. Hoboken, NJ, USA: Wiley, 2004.
[29] M. Strantza *et al.*, "Feasibility study on integrated structural health monitoring system produced by metal three-dimensional printing," *Struct. Health Monit.*, vol. 14, no. 6, pp. 622–632, Nov. 2015.
[30] M. Strantza *et al.*, "Fatigue of Ti6Al4V structural health monitoring systems produced by selective laser melting," *Materials*, vol. 9, no. 2, p. 106, Feb. 2016.
[31] S.-Y. Wu, C. Yang, W. Hsu, and L. Lin, "3D-printed microelectronics for integrated circuitry and passive wireless sensors," *Microsyst. Nanoeng.*, vol. 1, Jul. 2015 Art. no. 15013.
[32] L. Yang, O. Harrysson, H. West, and D. Cormier, "Mechanical properties of 3D re-entrant honeycomb auxetic structures realized via additive manufacturing," *Int. J. Solids Struct.*, vols. 69–70, pp. 475–490, Sep. 2015.

Michaël Hinderdael received the M.Sc. degree in mechanical engineering from Vrije Universiteit Brussel (VUB) and Université Libre de Bruxelles (ULB), Brussels, Belgium, in 2014, and the Ph.D. degree in engineering from VUB, in 2018.

He is with the Department of Mechanical Engineering, VUB, where he is still active as a Post-Doctoral Researcher. His current research focuses on embedded structural health monitoring solutions for additively manufactured components.

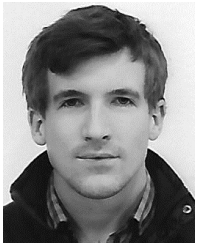

Marc Moonens received the degree in electromechanical engineering from the Université Libre de Bruxelles (ULB) in 2014.

He then started working in the shipbuilding industry, where he was involved in the design and construction of a jack-up vessel. In 2017, he became a Research Assistant at the Mechanical Engineering Department, Vrije Universiteit Brussel (VUB), a position which he still occupies. His main research interests are the fracture mechanics behavior of additively manufactured metals with a particular focus on the fatigue crack propagation behavior.

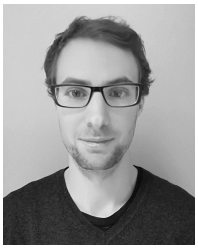

Julien Ertveldt received the degree of Industrial Engineer in electromechanics from the Erasmus University College, Brussels, Belgium, in 2011, the M.Sc. degree in aerospace vehicle design from Cranfield University, U.K., in 2013, and the Ph.D. degree in engineering from Vrije Universiteit Brussels (VUB), Belgium, in 2017. Since 2018, he has been a Research Engineer at the VUB Department of Mechanical Engineering, where he is involved in the development of controlled additive manufacturing solutions.

Dieter De Baere received the master's degree in industrial sciences and technology in electromechanical engineering from the Katholieke Hogeschool Brugge-Oostende, Ostend, Belgium, in 2004, and the M.Sc. degree of electro-mechanical engineering in aeronautics from Vrije Universiteit Brussel (VUB), Brussels, Belgium, in 2006.

From 2006 to 2012, he worked as a Test and Development Engineer at Asco Industries. In 2012, he joined the Department of Mechanical Engineering, VUB, as a Ph.D. Researcher.

Patrick Guillaume received the M.Sc. degree in mechanical-electrotechnical engineering and the Ph.D. degree from Vrije Universiteit Brussel (VUB), Brussels, Belgium, in 1987 and 1992, respectively.

In 1987, he joined the Department of Electrical Engineering, VUB. Dr. Guillaume joined the Department of Mechanical Engineering, VUB, in 1996, where he is currently a Lecturer.